



A Non-destructive Rapid Assessment of Blue Carbon Sequestration Potential in Mangrove Forests of the Red Sea Region

Esraa Aziz El-Masry

Oceanography Department, Faculty of Science, Alexandria University, Alexandria, Egypt

*Corresponding Author: esraaelmasry@alexu.edu.eg

ARTICLE INFO

Article History:

Received: Jan. 16, 2024

Accepted: Jan. 27, 2024

Online: Feb. 4, 2024

Keywords:

Above ground biomass (AGB),
Below ground biomass (BGB),
Allometric equation,
Remote sensing,
Avicennia marina

ABSTRACT

Non-destructive approaches for estimating the carbon sequestration potential of mangroves are growing in acceptance, as they are eco-friendly and do not harm trees. The present study was piloted for mangroves, especially the *Avicennia marina* of the Red Sea region. The study aimed to use allometric models for mangrove biomass estimation based on the normalized difference vegetation index (NDVI) derived from satellite imagery. The method was validated by comparing the results with the previous studies that adopted the destructive method. To achieve the study aim, three major steps were adopted; namely, (1) Mangrove mapping using satellite imagery, (2) Calculation of carbon sequestration potential by applying the allometric equations, and (3) Mangrove sediments sampling and analysis were carried out in three stations along the Egyptian coast to determine soil organic carbon stock. Results from the study revealed that mangroves grew at 56 locations along the Red Sea coast. The results of the present study showed that the average carbon stock value for the Red Sea mangroves was 0.33 (ton C/ hectare) (1.2 ton CO₂/ hectare). Thus, the Red Sea mangroves can share by at least USD 27.5M value of mangrove forest ecosystem services. Middle station on the Saudi Arabia coast was found to be the most carbon-rich mangrove region with 26.9 ton C/ hectare, while one station in northern Egypt recorded the lowest carbon sequestration potential, with a total carbon stock of 0.06 ton C/ hectare. Therefore, the current study suggested that the satellite imagery analysis combined with allometric equations can be applied far more rapidly and inaccessibly compared to traditional field inventory techniques, and it can potentially be an effective tool for estimating mangrove biomass and carbon storage with increased accuracy through further model calibration.

INTRODUCTION

The recent and prominent Intergovernmental Panel on Climate Change (IPCC) Special Report on the Ocean and Cryosphere in a Changing Climate (SROCC) focused on the potential for coastal ecosystems to mitigate climate change and create co-benefits (Intergovernmental Panel on Climate Change (IPCC, 2022)). The carbon sequestration

capacity of these ecosystems, especially wetlands, has received great attention, and the carbon stored in their biomass and sediments is now commonly referred to as “blue carbon” (Hilmi *et al.*, 2021; Santos *et al.*, 2021; Wasserman *et al.*, 2023). Thus, blue carbon has drawn the interest of a wide range of players beyond the scientific community at the local, national, regional, and global levels to evaluate their contribution at larger scales in order to meet policymakers’ requirements (Taillardat *et al.*, 2018; Wasserman *et al.*, 2023).

Mangroves represent 31% of the total worldwide blue carbon ecosystems (Ahmed & Glaser, 2016). In addition, mangroves can store up to five times as much carbon as tropical forests do per unit area. Palacios Peñaranda *et al.* (2019) stated that they can capture approximately 24Tg C/ year and sequester over 2 tons of carbon on an average per ha/ year. However, these ecosystems rapidly degrade, limiting their ability to store carbon and probably convert them to carbon dioxide sources (Rovai *et al.*, 2021). Since the 1980s, more than 35 percent of the mangrove area has diminished, and mangroves are gravely threatened (Curnick *et al.*, 2019).

Mangrove habitats may store carbon by producing both above- and below-ground biomass, which can be used to assess carbon sequestration. The carbon stored in all biomasses of living vegetation is known as the above-ground biomass, whereas that stored in the sediments of mangrove ecosystems is known as the below-ground carbon storage (Suwa *et al.*, 2021).

Accurate methods for estimating the biomass of mangroves and their stored carbon are necessary for managing mangrove ecosystems for climate mitigation, adaptation, and related services (Hickey *et al.*, 2018). The carbon sequestration potential of mangrove stands has been estimated using destructive and non-destructive methods (Wijeyaratne & Liyanage, 2022). The destructive method of estimating carbon sequestration potential depends on the removal of the tree from its native habitat to determine the carbon content of the plant parts. Accordingly, this method is not environmentally friendly, expensive, and time-consuming (Ross *et al.*, 2001; Soares & Schaeffer-Novelli, 2005; Kauffman & Cole, 2010). Additionally, it is usually restricted to small plots that might not be representative of an entire forest (Hickey *et al.*, 2018; Wijeyaratne & Liyanage, 2022). On the other hand, the non-destructive method involves simulating the capacity for carbon storage by creating allometric equations using quantifiable tree measurements (Soares & Schaeffer-Novelli, 2005; Subasinghe *et al.*, 2014; Hickey *et al.*, 2018).

However, the requisite point measurement input parameters might be challenging to collect; Saenger and Snedaker (1993) created an allometric equation for mangroves that is worldwide and applicable to all species. These equations give a way to estimate

biomass across the vast scales needed to monitor mangrove changes since tree height can be determined with remote sensing techniques (Jones *et al.*, 2020). Situmorang *et al.* (2016) recorded a significant correlation ($R^2 = 0.729$) between the estimated carbon stock derived from an allometric equation and the vegetation index derived from satellite data. This high determination coefficient suggests that estimating carbon stock using satellite data is possible. Numerous studies estimate mangrove biomass using various satellite sensors (Rosenqvist *et al.*, 2014; Pham & Brabyn, 2017; Dou *et al.*, 2018; Hickey *et al.*, 2018; Vaghela *et al.*, 2021; Meng *et al.*, 2022; Xu *et al.*, 2023). However, due to variations in spatial, temporal, and spectral resolution, as well as variable imaging techniques (active and passive), these sensors exhibit notable disparities in the accuracy of biomass estimation (Pham & Brabyn, 2017; Vaghela *et al.*, 2021).

Thus, the present study is an early attempt to evaluate the capability of the Red Sea mangrove for carbon sequestration using a rapid non-destructive method in addition to the valuation of the mangrove blue carbon for the Red Sea region. Although light detection and ranging (LiDAR) is an active sensor using a laser pulse to measure the height and shape of an object (tree), as is often the case, the actual (LiDAR) data do not fully cover the extent of tiles that are on the perimeter of the Red Sea region. Khalil (2015) reported that AGB estimates of *Avicennia marina* in the Red Sea region are readily compared with other communities of similar heights. Additionally, he suggested that, despite the climatic constraints, mangrove standing stock in the Red Sea is similar to other regions. Komiyama *et al.* (2008) assumed that, the allometric equations of biomass estimation for mangrove species are substantially species-specific but less site-specific. This recommendation is supported by the findings of Owers *et al.* (2018) and Kauffman and Donato (2012), who identified spatial variability in both biomass and carbon storage in *A. marina* and other mangroves based on structure and growth form.

Therefore, this study aimed to establish proof-of-concept for the rapid assessment of the biomass of mangrove stands, using the data derived from Landsat 8 OLI /TIRS, which resolves the mangrove horizontal extent, relying on normalized difference vegetation index (NDVI), and the generic allometric equations previously developed for the same mangrove species in a different region for biomass estimation to determine where areas of low and high biomass occur in the Red Sea region as a pilot area for the adoption of this non-destructive method. Then, to verify this approach, the findings were compared to those of earlier research conducted in the Red Sea region.

MATERIALS AND METHODS

1. Study area

The study was carried out along the Red Sea coast (Fig. 1), which borders Egypt, Sudan, Eritrea, Saudi Arabia, and Yemen. The region has humid tropical to subtropical

weather. Seasonal variations in sea surface temperatures range from 22 to 32°C, with a high latitudinal gradient (**Berumen et al., 2019**) but limited longitudinal fluctuation (**Shaltout et al., 2020**). Salinity ranged from 36 (northern part) to 41 (southern part) practical salinity units (PSU) (**Blanco-Sacristán et al., 2022**). These high salinity ranges are caused by the hot air and water temperatures, little precipitation, considerable evaporation, and the lack of freshwater sources.

The Red Sea is near the northern limit of mangroves in the Indo-Pacific region, situated in the Sinai Peninsula at 28°N. Mangroves are present in the form of fragmented stands in many tidal areas of the Red Sea coast. They consist mainly of *Avicennia marina* trees accompanied by a few *Rhizophora mucronata*, however it is very rare (**PERSGA/GEF, 2004**). Mangroves in the Red Sea may not be as lush as those on other tropical shores; however, they play crucial ecological roles. Similar to other mangrove ecosystems, they are nurseries for several commercial fish species, and they protect coral reefs by trapping sediment loads from the seasonal rainwater influx (**PERSGA/GEF, 2004**). Due to excessive cutting, camel over-browsing, damming of rainwater draining through valleys, pollution, and coastal constructions, mangroves have reportedly degraded in several areas of the region (**Almahasheer et al., 2016**). Nevertheless, due to restoration and reforestation initiatives, the total area of the Red Sea mangroves (135 km²) has grown by 12 % over the past forty years (**Blanco-Sacristán et al., 2022**). For this reason, it is essential to develop and establish approaches that precisely track mangrove extent, density, and ultimately carbon storage to provide information that may be used to support management intervention, conservation, and potential for restoration.

Mangroves typically develop as thin or, rarely, dense forests along the shoreline, on near and offshore islands, and fringing tidal creeks and channels of various sizes (**PERSGA/GEF, 2004; Afefe, 2021**). The Red Sea mangroves are endangered due to the following issues (**PERSGA/GEF, 2004**):

- Camel grazing causes a reduction in the green parts, limiting the tree growth to stunted multi-stemmed bushes, and destruction of the seedlings and pneumatophores.
- Rapid coastal development involves dredging and sediment dumping on the shore; diversion of tidal water through newly constructed canals to feed salt pans, and excessive sedimentation by sand dunes that have buried and closed some of the tidal channels through which seawater flows into the mangroves.
- Pollution in the mangrove areas (domestic solid waste and oil pollution)
- Aquaculture projects pose a serious threat to the mangroves through water quality degradation and the consequent spread of diseases.

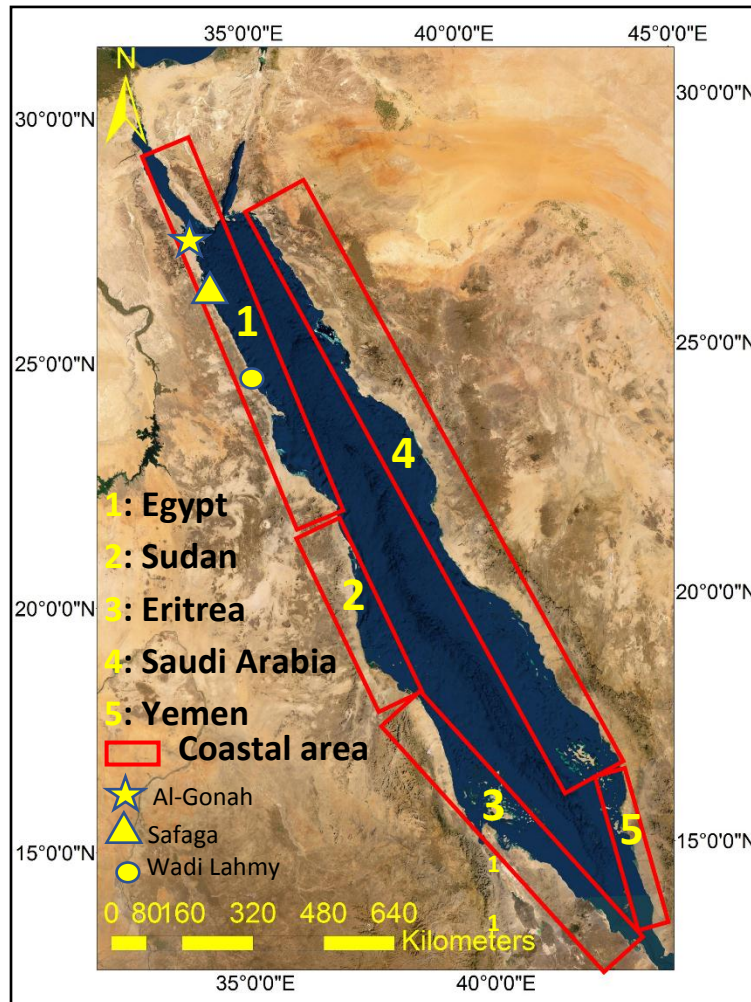


Fig. 2 The map of the study area showing the five studied locations and the sampling station (for Egypt).

Some studies have been carried out to evaluate the carbon sequestration potential (CSP) of mangrove forests along the Red Sea coast, especially in Saudi Arabia and Egypt as follows:

- a) **Saudi Arabia:** Only one study was conducted in a central location along the Saudi Arabian coast; the others were all done in southern areas. **Eid *et al.* (2016, 2020)** and **Shaltout *et al.* (2020)** studied the efficiency of mangrove forests in carbon sequestration and determined soil organic carbon (SOC) pools for the southern Saudi Arabian Red Sea coast. **Almahasheer *et al.* (2017)** evaluated the sediment organic carbon (C_{org}) stocks, and sediment Corg sequestration of mangroves along the Central Red Sea. **Arshad *et al.* (2018)** explored the vertical distribution of the sediment bulk density (SBD), sediment organic carbon (SOC) concentration, and carbon sequestration rate (CSR) in two polluted mangrove

locations in comparison, with a non-polluted location along the southern Red Sea coast of Saudi Arabia.

- b) **Egypt: El-Hussieny and Ismail (2015), Eid and Shaltout (2016), and Mashaly *et al.* (2016)** investigated the carbon sequestration potential of mangrove forests in different locations along the Red Sea coast of Egypt. In addition, **Afele *et al.* (2020)** quantified the carbon storage (above- and below-ground) in the biomass and sediment of mangrove forests and estimated the carbon sequestration potential in the Gebel Elba Protected Area along the Egyptian African Red Sea coast.

All the previous studies were concerned with the Red Sea mangroves; yet, no research has assessed the blue carbon stock of mangrove vegetation in the whole Red Sea region.

This study determined the mangrove forest extent from Landsat 8 OLI through (NDVI) values. Due to the inability to get the LiDAR data for the study area to obtain the tree height and site-specific allometric model in each site was not available, the present study used the generic allometric equations for (AGB) and (BGB) determination in the subtropical region. The spatial distribution of mangrove stands and their carbon sequestration potential were determined following the methodological framework adopted by the present study (Fig. 2).

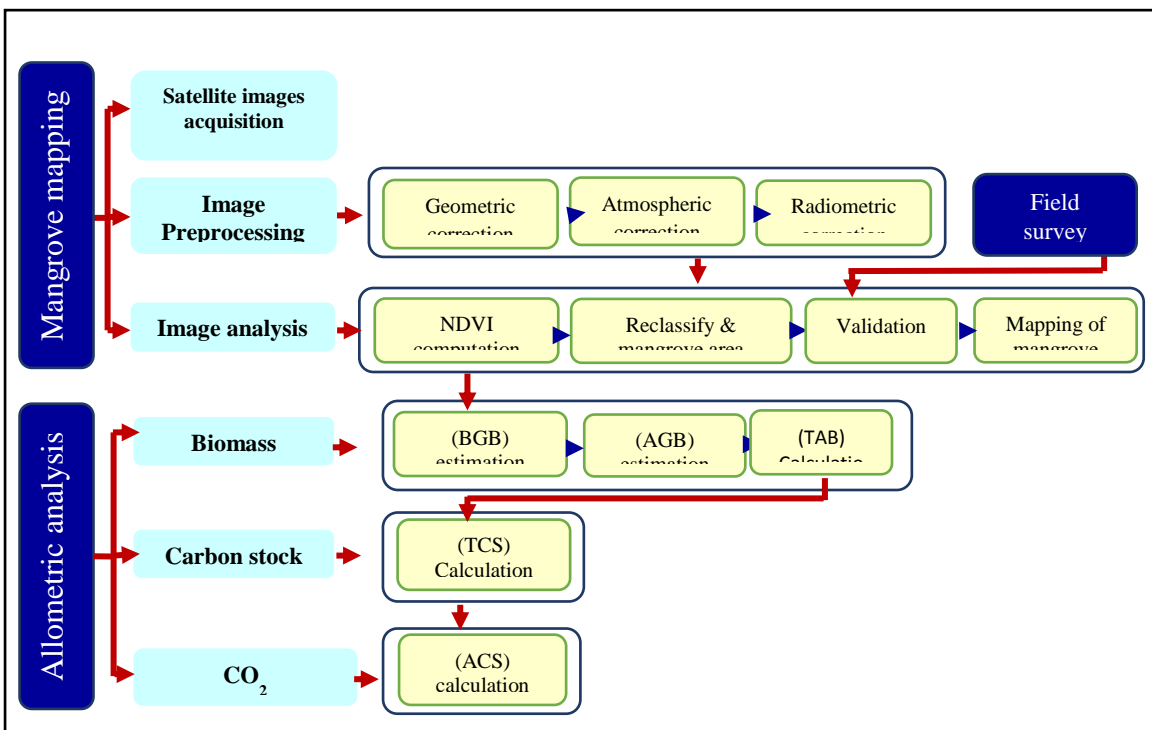


Fig. 2. Methodological framework adopted in the present study for determining the carbon sequestration potential in the Red Sea mangroves

Data sets

Data required for this study were obtained from the United States Geological Survey (USGS) through the website <https://earthexplorer.usgs.gov>. Twenty satellite images with 15m spatial resolution covering the Red Sea region employed in the present study are presented in Table (1). To eliminate the effects of seasonal variations, all images were selected to be taken on or very close to the purchase dates. The USGS corrected all the landsat images, with a total root-mean-square error of less than 0.4m. The landsat images were chosen to be of good quality (IQ= 9) and cloud-free (less than 10%).

2. Remote sensing and geographic information system (GIS) applications

2.1 Image preprocessing

The pre-processing of the satellite image includes geometric correction, radiometric correction for converting digital number (DN) values to surface reflectance, and an atmospheric correction to the data in which the pixels were converted to top of atmosphere (TOA) spectral radiances using the radiance rescaling factors provided in the metadata file.

Table 1. Satellite images used in the present study

Country	Satellite/ sensor	Path/ row	Acquisition date (dd/mm/yy)
Egypt	Landsat 8 (OLI/TIRS)	173/43	22/07/2022
	Landsat 8 (OLI/TIRS)	174/41	29/07/2022
	Landsat 8 (OLI/TIRS)	174/42	29/07/2022
Sudan	Landsat 9 (OLI-2/TIRS-2)	170/47	23/06/2022
	Landsat 8 (OLI/TIRS)	171/46	26/06/2022
	Landsat 8 (OLI/TIRS)	171/47	06/06/2022
Eritrea	Landsat 8 (OLI/TIRS)	167/50	10/06/2022
	Landsat 8 (OLI/TIRS)	167/51	26/06/2022
	Landsat 9 (OLI-2/TIRS-2)	168/50	25/06/2022
	Landsat 8 (OLI/TIRS)	169/49	24/06/2022
Saudi Arabia	Landsat 9 (OLI-2/TIRS-2)	167/49	04/07/2022

	Landsat 9 (OLI-2/TIRS-2)	169/46	18/07/2022
	Landsat 8 (OLI/TIRS)	170/44	25/07/2022
	Landsat 8 (OLI/TIRS)	170/45	17/07/2022
	Landsat 8 (OLI/TIRS)	170/46	17/07/2022
	Landsat 8 (OLI/TIRS)	171/43	24/07/2022
	Landsat 8 (OLI/TIRS)	172/42	31/07/2022
	Landsat 9 (OLI-2/TIRS-2)	173/41	30/07/2022
Yemen	Landsat 8 (OLI/TIRS)	166/50	05/07/2022
	Landsat 9 (OLI-2/TIRS-2)	166/51	29/07/2022
	Landsat 9 (OLI-2/TIRS-2)	167/48	04/07/2022
	Landsat 9 (OLI-2/TIRS-2)	167/49	04/07/2022

2.2 Normalized difference vegetation index (NDVI)

The normalized difference vegetation index (NDVI) is the most extensively used remote sensing-based proxy for vegetation monitoring (**Panda et al., 2010**). The NDVI was calculated using the equation implemented by **Kovacs et al. (2004)**, as follows:

$$(NDVI) = \frac{(NIR)-(RED)}{(NIR)+(RED)} \quad 1$$

Where, NIR is the reflectance radiated in the near-infrared wave band, and RED is the reflectance radiated in the visible red wave band of the satellite radiometer. The value of NDVI ranges from -1 to 1, representing the reaction to the photosynthetic activity; the higher the (NDVI) value, the greater the vegetation cover (**Lin et al., 2006**).

Mangroves are the only significant vegetation along the Red Sea coast since it is surrounded by a desert. This means that the classification problem is limited to the presence/absence of vegetation. Mangrove tree density was evaluated using (NDVI) estimates. Moreover, the (NDVI) class values were reclassified into three classes: the rare, medium, and dense classes.

2.3 Estimation of biomass, carbon stock, and carbon dioxide (CO₂) sequestration potential

The biomass, carbon stocks, and carbon sequestration are calculated by constructing the equations presented in Table (2) (Equations 2- 6), using ArcGIS

geoprocessing toolbox application for landsat image 8, following the method developed by **Hastuti et al. (2017)**. The term "biomass" refers to the combined dry weight of both the above-ground biomass (AGB) and the below-ground biomass (BGB), including wood, bark, branches, twigs, stumps, and roots, as well as the dead mass of soil-associated litter (**Pizaña et al., 2016**). Allometric equations were used as a non-destructive means of (AGB) estimation, using field-measured parameters available for mangrove forests (**Rasquinha & Mishra, 2021**). The total carbon stock of the mangrove stand is estimated from the total accumulated biomass (organic carbon (OC)% for mangrove biomass is 0.47, as indicated by **Kauffman and Donato (2012)**, and then the converted amount of CO₂ sequestration was calculated according to the equation developed by **IPCC (2001)**.

Table 2. Allometric equations employed in the present study

Index		Equation	Reference
Biomass	Above ground biomass (AGB)	$(AGB)(\text{ton/ ha}) = 305.9 * (NDVI)^{4.864}$ 2	Jha et al. (2015)
	Below ground biomass (BGB)	$(BGB)(\text{ton/ ha}) = e^{(-1.0587+0.8836*\ln(AGB))}$ 3	Cairns et al. (1997)
	Total accumulated biomass (TAB)	$(TAB)(\text{ton/ ha}) = (AGB) + (BGB)$ 4	Hogarth (2002)
Total carbon stock (TCS)		$(TCS)(\text{tonC/ ha}) = (TAB) * \%OC$ 5	(Westlake, 1963)
Amount of CO ₂ sequestration (ACS)		$(ACS)(\text{tonC/ ha}) = (TCS) * 3.67$ 6	(IPCC, 2001)

3. Statistical analysis

The statistical analysis, data calculations, and illustrations of the biomass estimation, TSC, and ACS were carried out using the raster calculator toolbox in ArcGIS 10.8, following the equations displayed in Table (2)

3.1 Determination of mangrove sediment characteristics for Egypt

During the summer of 2022, three stations (Al-Gonah, South Safaga, and Wadi Lahmy) were selected for the sediment sampling to represent the mangrove forests along the Egyptian Red Sea coast (Fig. 1). In each of the sampling stations, three cores were collected (3.5 inches in diameter and 30cm in length), 2 from the mangroves area and one from the reference area (non-mangrove area). Cores were immediately refrigerated, divided into 2 halves, and each half was sliced into 5cm intervals, then preserved in labeled sterilized plastic bags until the analysis was done as shown below, and the calculation was carried out on Microsoft Excel 365.

4. Sediment texture analysis

The textual characteristics of the sediments were determined using the sieving technique according to López (2017). Grain Size Analysis. In: Gilbert, A.S. (eds) Encyclopedia of Geoarchaeology. Encyclopedia of Earth Sciences Series. Springer, Dordrecht. https://doi.org/10.1007/978-1-4020-4409-0_18. Fifteen grams of the oven-dried samples were subjected to grain size analysis. The mechanical technique was employed for coarse fractions (less than 4Ø) by sieving on test sieve shaker for 20 minutes. The sieves were arranged at 1Ø class intervals from top to bottom.

The grain size analysis results using phi notation, where $\phi = -\log^2 d$ (d given diameter value in mm), were represented graphically. On a probability paper, cumulative percentages were plotted against the grain size interval (Ø). The values of 5, 16, 50, 84, and 95 were interpolated from the cumulative curves. The inclusive graphic mean size (Mz) and inclusive graphic standard deviation (sorting, σ_1) were computed (Equations 7 and 8).

$$\text{Inclusive graphic mean size (Mz)} = (\phi_{16} + \phi_{50} + \phi_{84}) / 3 \quad 7$$

$$\text{Inclusive graphic standard deviation } (\sigma_1) = (\phi_{84} - \phi_{16} / 4) + (\phi_{95} - \phi_5 / 6.6) \quad 8$$

4.1 Determination of sediment organic carbon (SOC) stock

The SOC stock was calculated using equation 9 following the method developed by Howard *et al.* (2014), as follows:

$$\text{SOC (tonC/ha)} = \text{Bd} \times \text{H} \times \text{OC} \quad 9$$

Where, SOC is the sediment organic carbon stock (ton C/ha); OC is the organic carbon concentration (%); Bd is the bulk density (g/ cm³), and H is the sediment thickness (cm).

Therefore, to calculate SOC stock for the mangrove stand, SBD and OC were determined first as follows:

i) Determination of sediment bulk density (SBD)

To determine the SBD as presented in equation 10, samples were oven-dry at 105°C for three days, cooled down to room temperature in a desiccator, and weighed, as presented below **Wilke (2005)**:

$$P_{sj} = m_j/v_j \quad 10$$

Where, P_{sj} is SBD (g/cm^3) of the j^{th} layer; m_j is the mass of soil sample (g) of the j^{th} layer dried at 105°C, and v_j is the volume of soil sample (cm^3) of the j^{th} layer. Dry samples were be ground and sieved to pass through 2mm particle size.

ii) Determination of organic carbon content

The organic carbon content was determined by the method explained by **Sidi et al. (2023)**. About 200 grams of dry sediment sample was oxidized by 10ml of chromic acid in a boiling tube and heated in a water bath for 15 minutes. After the sample was cooled, it was poured into distilled water, and titrated against ferrous ammonium sulphate using the phenanthroline indicator until the pink color persisted (Equation 11).

$$1\text{ml } 0.2 \text{ ferrous ammonium sulphate} \equiv 1.15 \times 0.6\text{mg organic carbons} \quad 11$$

RESULTS AND DISCUSSIONS

1. Mangrove distribution along the Red Sea coast

The normalized difference vegetation index (NDVI) was used to identify mangrove distribution in the Red Sea region. Fifty-six mangrove stands were identified, and the individual mangrove extent maps of Egypt, Sudan, Eritrea, Saudi Arabia, and Yemen were generated (Table 3 & Fig. 3). Based on NDVI reclassification process, the lowest value was detected in Egypt (station 3- Marsa Abu Zabad) (0.19). The extremely saline base underneath is primarily characterized by low-growing shrubs (**PERSGA/GEF, 2004**). The maximum vegetation density value was identified in Saudi Arabia (station #36-Al-Badeaa) (0.68), which may be attributed to the location of the dense stance in a sheltered bay. The average NDVI value for the Red Sea is 0.25, which is a small value that may be due to the lack of freshwater and soil inputs, leading to acute nutrient limitation of Red Sea mangroves (**Almahasheer et al., 2017**). The mangrove occurrence and distribution are limited by different factors, such as geomorphology, soil characteristics, water salinity, and nutrient availability (**Wilson et al., 2009**).



Fig. 3. Distribution of the mangrove stands along the Red Sea (The station number of the mangrove stands is detailed in Fig. 9)

Table 3. Location of mangrove stands identified in the Red Sea coast

Country	Station no.	Station name	Location
Egypt	1	Shura Al-Rwaisat	28°12'N, 34°25'E
	2	Shura Al-Manquata	28° 12.5'N, 34° 25'E
	3	Marsa Abu Zabad	28° 09'N, 34° 27'E
	4	Shura Al-Gharqana	28° 07'N, 34° 26.5'E
	5	Ras Muhammed	27°43'N, 34°14'45'E
	6	Geisum Island	27° 40'N, 33° 42'E
	7	Al-Gonah	27° 24'N, 33° 41'E
	8	Abu Minkar Island	27° 13'N, 33° 52'E
	9	Safaga Island	26° 45'N, 33° 59'E

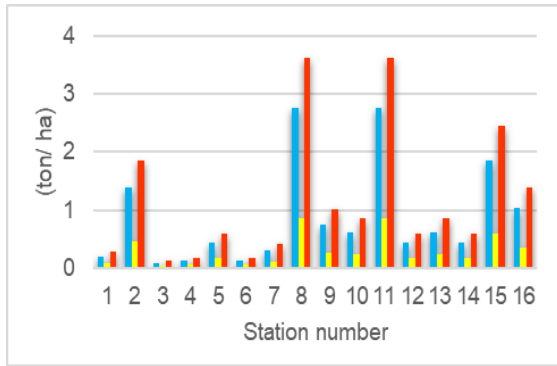
	10	South Safaga	26° 38'N, 33° 59'E
	11	Wadi Abu Hamra	26° 21'N, 34° 09'E
	12	Sharm El-Bahari	25° 52'N, 34° 24'E
	13	Sharm El-Qebli	25° 50'N, 34° 26'E
	14	Wadi El-Gimal	24° 40'N, 35° 05'E
	15	Wadi Lahmy	24° 13'N, 35° 26'E
	16	Marsa El-Hamira	23° 29'N, 35° 29'E
Sudan	17	Mohammed Qol	20° 47'N, 37° 10'E
	18	Klanieb	19° 30'N, 37° 16'E
	19	Mersa Atta	19° 18'N, 37° 18'E
	20	Fagum-Lagagengeeb	19° 01'N, 37° 23'E
	21	Arkaweit	18°46'N, 37°25'E
	22	Ashat	18° 45'N, 37° 30'E
Eritrea	23	Dankalia	13°11'N, 42°33'E
	24	North Gelaalo	15°11'N, 40°4'E
	25	South Gelaalo	14°58'N, 40°25'E
	26	Arata	14°50'N, 40°44'E
	27	Afabet	16°35'N, 39°9'E
	28	Mitsiwa	15°37'N, 39°27'E
Saudi Arabia	29	Duba Sealake	27°25'N, 35°36'E
	30	Duba	27°19'N, 35°40'E
	31	Zabaid Island	26°54'N, 36°1'E
	32	Al-Wajh	26°38'N, 36°13'E
	33	Yanbu	23°56'N, 38°16'E
	34	Aiqa	22°1'N, 38°57'E
	35	Al-Qadeimah Port	22°20'N, 39°6'E

	36	Al-Badeaa	21°15'N, 39°7'E
	37	Al-Mahjar	21°24'N, 39°11'E
	38	Bahra	20°44'N, 39°27'E
	39	Al-Lith 1	20°32'N, 39°37'E
	40	Al-Lith 2	20°14'N, 40°4'E
	41	Rake	20°9'N, 40°13'E
	42	Ras Umrubis	20°3'N, 40°23'E
	43	Umrubis Island	19°39'N, 40°45'E
	44	Farasan	16°47'N, 41°58'E
Yemen	45	Midi	16° 21'N, 42° 47'E
	46	Between Midi and Al-Habl	16° 15'N, 42° 48'E
	47	Al-Habl	16° 09'N, 42° 49'E
	48	Al-Buhays	15° 59'N, 42° 49'E
	49	Between Al-Buhays and Al-Luhayah	15° 49'N, 42° 46'E
	50	Al-Luhayah	15° 42'N, 42° 41'E
	51	Ibn Abbas	15° 29'N, 42° 46'E
	52	Al-Harounia mersa	15° 18'N, 42° 48'E
	53	Kamaran Island	15° 22'N, 42° 35'E
	54	Al-Urj	15° 06'N, 42° 52'E
	55	Al-Hudaydah	14° 53'N, 42° 56'E
	56	El-Ghurairah	12° 44'N, 43° 28'E

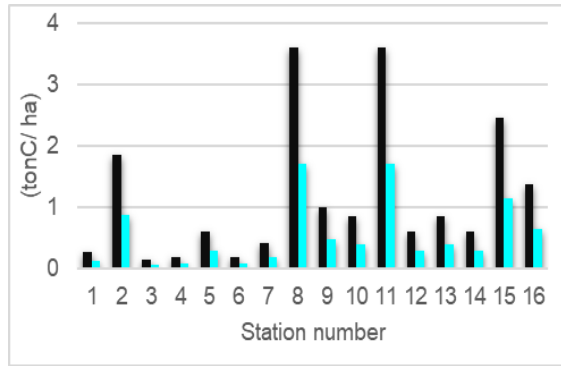
2. Biomass, carbon stock (TCS) and amount of CO₂ sequestration (ACS) potential assessment

The results of the biomass analysis (AGB, BGB, and TAB) and carbon stock for the selected mangrove stations are presented in Fig. (4) and Tables (4, 5).

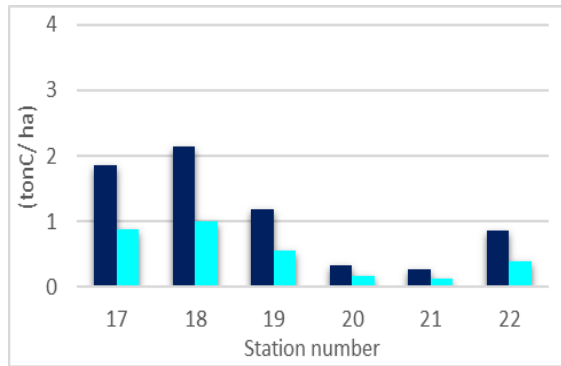
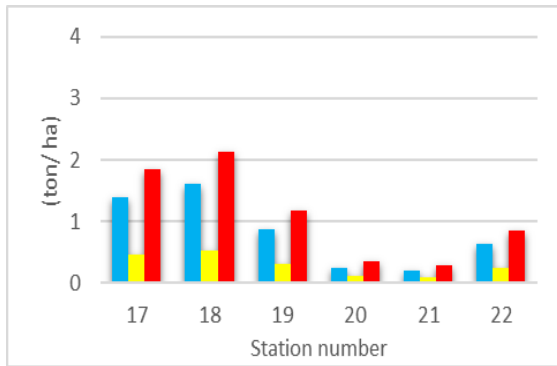
A



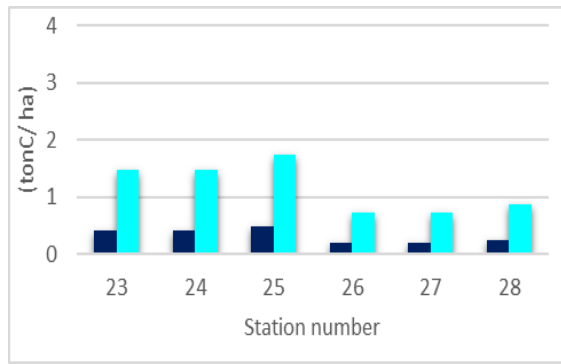
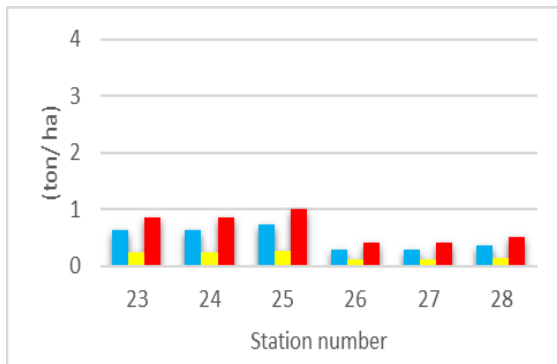
B



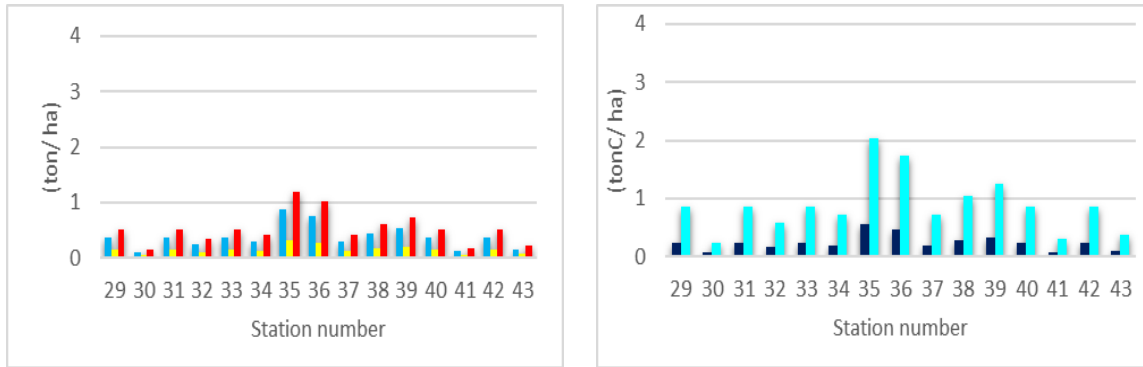
Egypt



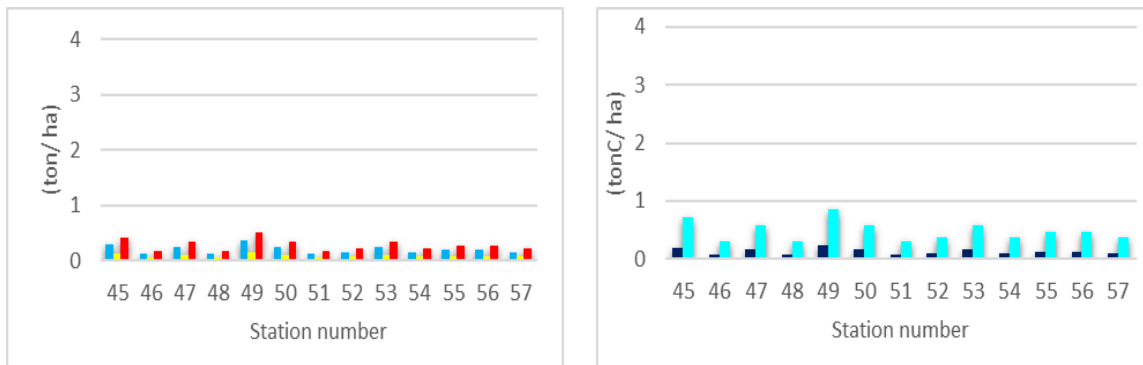
Sudan



Eritrea



Saudi Arabia



Yemen

Fig. 4. A. Average values of (AGB ■), (BGB ■), and (TAB ■) (Biomass indices) (ton/ha), and **B.** Average values of (TCS ■) (ton C/ha), and (ACS ■) (ton CO₂/ha), for each country

Table 4. Estimation of AGB, BGB, and TAB for the studied countries

Country	(AGB)(ton/ ha)			(BGB)(ton/ ha)			(TAB)(ton/ ha)		
	Min.	Max.	Aver.	Min.	Max.	Aver.	Min.	Max.	Aver.
Egypt	0.09	13.95	0.87	0.04	3.56	0.29	0.14	17.51	1.16
Sudan	0.19	8.61	0.82	0.08	2.33	0.29	0.28	10.94	1.11
Eritrea	0.30	10.50	0.49	0.12	2.77	0.18	0.41	13.28	0.67
Saudi-Arabia	0.09	46.87	0.37	0.04	10.39	0.14	0.14	57.26	0.51
Yemen	0.12	8.61	0.20	0.05	2.33	0.08	0.18	10.94	0.28

2.1 Biomass

The estimated average AGB of the Red Sea mangroves ranged from 0.09 ton/ ha in Egypt (station 3- Marsa Abu Zabad) and Saudi Arabia (station 30-Duba) to 2.7 ton/ ha in Saudi Arabia (station 36-Al-Badeaa), with an average value of 0.53 ton/ ha.

Table 5. Estimation of TCS and ACS for the studied countries

Country	TCS (ton C/ ha)			ACS (ton CO ₂ /ha)		
	Min.	Max.	Aver.	Min.	Max.	Aver.
Egypt	0.06	8.23	0.55	0.24	30.20	2.01
Sudan	0.13	5.14	0.52	0.47	18.87	1.91
Eritrea	0.19	6.24	0.32	0.71	22.90	1.16
Saudi-Arabia	0.06	26.91	0.24	0.24	98.77	0.88
Yemen	0.08	5.14	0.13	0.30	18.87	0.48

The wide variation in AGB in individual plots is attributed to the differences in species composition, age, tree density, phenological condition of the trees at the time of satellite data acquisition, and selection of allometric equations (Jha *et al.*, 2015). The calculated (BGB) values were 0.04 ton/ ha in Egypt (station#2-Shura Al-Manquata), and 10.39 ton/ ha in Saudi-Arabia (station#36-Al-Badeaa), with an average of 0.19 ton/ ha. The BGB values in all studied mangrove stands were lower than those of above-ground mangrove components. According to Donato *et al.* (2011), the BGB of mangrove ecosystems is 4– 18 times larger than that of tropical rainforests. Meng *et al.* (2021) mentioned that the BGB values are usually lower than those of the above ground. Jaramillo *et al.* (2011) found that the BGB value was lower than the AGB component for tropical forests by 6%. This observation coincides with those recorded in several studies and different locations (Kauffman & Donato, 2012; Gao *et al.*, 2018; Cooray *et al.*, 2021).

The total accumulated biomass (TAB) is the total amount of biomass above and below the sediment surface (Wahyuning Hastuti *et al.*, 2017). The TAB lowest value was recorded in Egypt (station#3-Mersa Abu Zabad) (0.13 ton/ ha), and significantly the highest was detected in Saudi-Arabia (station#36-Al-Badeaa) (57.26 ton/ ha), with an average value of 0.27 ton/ ha.

2.2 Carbon stock (TCS) and amount of CO₂ sequestration (ACS) potential

The results of the TCS and ACS of the present study are presented in Table (5). The mangrove carbon stock is the quantity of carbon stored in mangroves (Wang *et al.*, 2019). The average carbon stock value for the Red Sea mangroves was 0.33 ton C/ ha and 1.2 ton CO₂/ ha. The carbon stock of Saudi Arabia (station#36-Al-Badeaa) was estimated to be 26.9 ton C/ ha and 98.7 ton CO₂/ ha, and was found to be the most carbon-rich mangrove region. Egypt (station#3-Mersa Abu Zabad) was the least carbon-rich area with a total carbon stock of 0.06 ton C/ ha and 0.2 ton CO₂/ ha.

Table (6) summarizes the previous work concerning AGB, BGB, TAB, and ACS for Egypt and Saudi Arabia. The findings revealed that the research regarding the Red Sea mangroves considered a variety of mangrove aspects (such as mangrove extent and distribution), but only a few recent studies determined the mangrove biomass and carbon sequestration potential. Table (6) shows the results obtained from a different location in Egypt (El-Hussieny & Ismail, 2015; Afele *et al.*, 2020; Ellatif *et al.*, 2022) and Saudi Arabia (Arshad *et al.*, 2018; Shaltout *et al.*, 2020) were within the range reported in the present study. The findings of the current study show that, even though earlier studies were based on destructive methods, forecasts made using non-destructive approaches are yielding outcomes that are comparable to those made using destructive methods.

Conversely, estimates obtained by Abohassan *et al.* (2012) for Saudi Arabia and Afele *et al.* (2020) for Egypt are higher than those calculated in the present study and also other previous studies on the same two regions.

Table 6. Summary of the previous work concerning AGB, BGB, TAB, and ACS for Egypt and Saudi Arabia (A: *Avicennia marina*, and B: *Rhizophora mucronate*)

Country	(AGB)	(BGB)	(TAB)	(TCS)	Station name	Reference
Egypt	-	-	-	0.03 – 1.06	South Sinai	(El-Hussieny & Ismail, 2015)
	-	-	-	31.96 - 120.15	South Sinai	(Mashaly <i>et al.</i> , 2016)
	45.9 (A)	22.4 (A)	7.6 (A)	30.81(A)	Sharm El Madfaa	(Afele <i>et al.</i> , 2020)
	3.83 (B)	18.3 (B)	2.2 (B)	25.2(B)	Marsa Sha'ab Marsa Abu Fassi	

				0.04	Egypt	(Afeife <i>et al.</i> , 2020)
	14.8	67.8	-	-	Yanbu, and Shuaiba	(Abohassan <i>et al.</i> , 2012)
Saudi-Arabia	-	-	-	0.9	Southern Coast	(Arshad <i>et al.</i> , 2018)
	-	-	-	0.60 – 0.95	Duba, Jeddah, El-Birk, Al-Shuquiq and Jazan	(Shaltout <i>et al.</i> , 2020b)

In similar conditions, **Aljenaid *et al.* (2022)** estimated carbon stocks in Bahrain mangroves (1.8 ton C/ ha), which is higher than the value (0.34 ton C/ ha) obtained in the present study. In addition, the carbon stock value, estimated in northwest China by **Yue *et al.* (2018)** (29.4 ton C/ha) and in Pakistan by **Khan *et al.* (2020)** (69.93 ton C/ha), is far more than the value determined in the present study. The carbon stock of mangrove ecosystems is therefore site-specific. It relies on the method adopted, latitudes, and topographical features that influence the community structure and the production of mangroves (**Senger *et al.*, 2021**). The relatively low carbon sequestration potential of the Red Sea mangroves may be attributed to the severe environmental conditions, such as little precipitation, nutrient limitation, and high temperature, declining the growth rates of the mangroves and increasing soil respiration rates (**Almahasheer, *et al.*, 2016**; **Almahasheer *et al.*, 2017**).

3. Trade-offs among allometric method and data obtained from the soil analysis in estimating carbon stock of mangrove stands (Egypt case study)

To compare the accuracy of the carbon stock acquired from satellite images using allometric models with the carbon stock obtained from the sediment analysis, Egypt was selected as a pilot station due to the accessibility of field visits. Results from core samples for the 3 selected stations are presented in Figs. (5- 7).

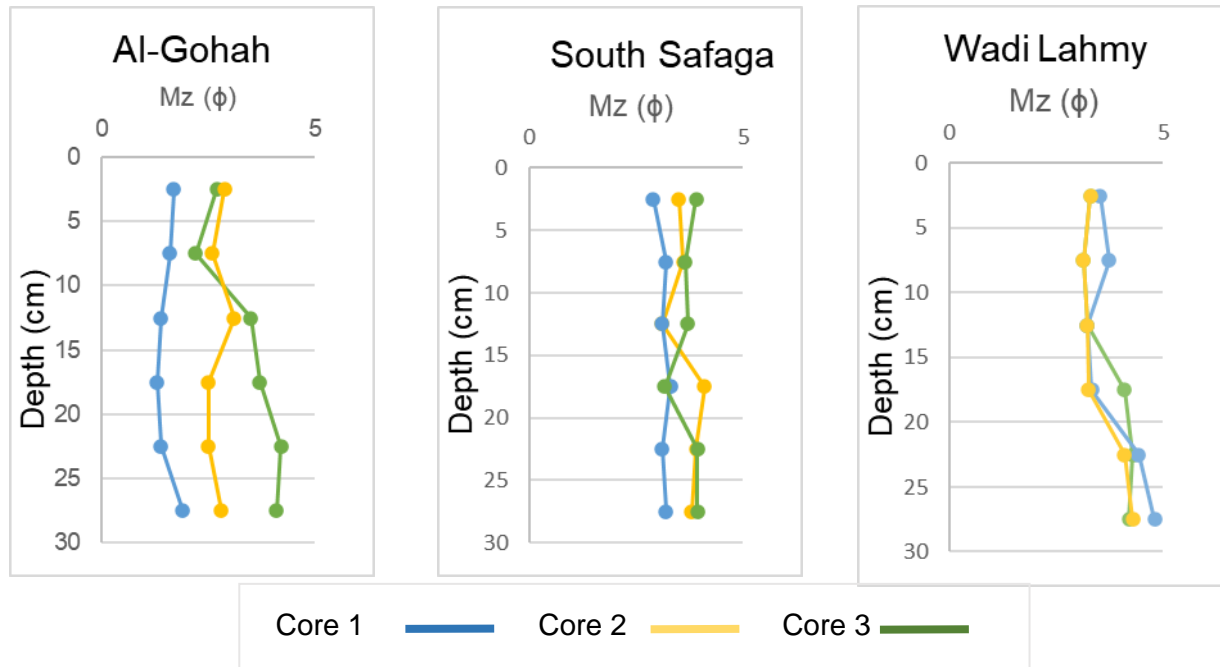


Fig. 5. Vertical distribution of the mean size (Mz Φ) in the sediment cores

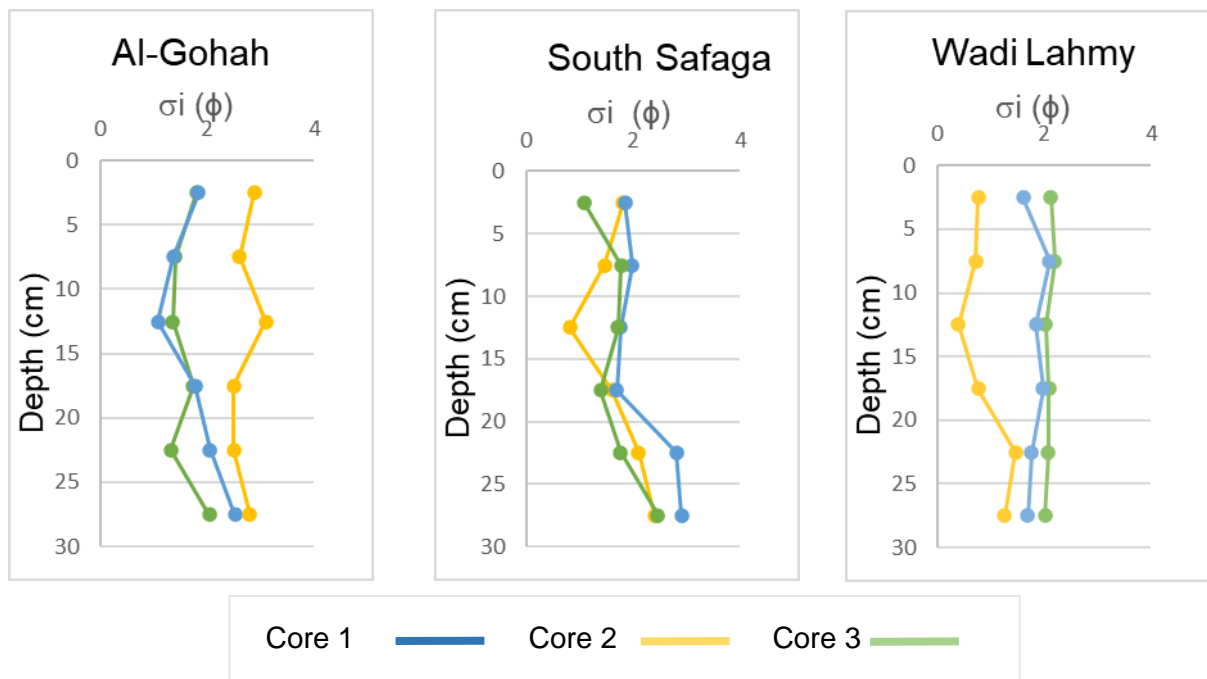


Fig. 6. Vertical distribution of the sorting ($\sigma_i \Phi$) in the sediment cores

Generally, the mean sediment grain size (Mz) was within the sand class, with an average value of $3.25 \pm 0.3\phi$, except for a few samples at the deepest layers of core 1 (Al-

Gonah), while cores 8 and 9 (Wadi Lahmy) were coarse silt, with an average value of $4.2 \pm 0.1 \phi$. Sediment in the 9 studied cores was poorly to very poorly sorted (average, 1.7 ± 0.5), which indicates the low energy environment, with quite an effective winnowing activity at the surface layers, with no effect on the deeper layers. These results agree with the findings of Madkour and Mohammed (2008), Afele *et al.* (2019) and Ellatif *et al.* (2022).

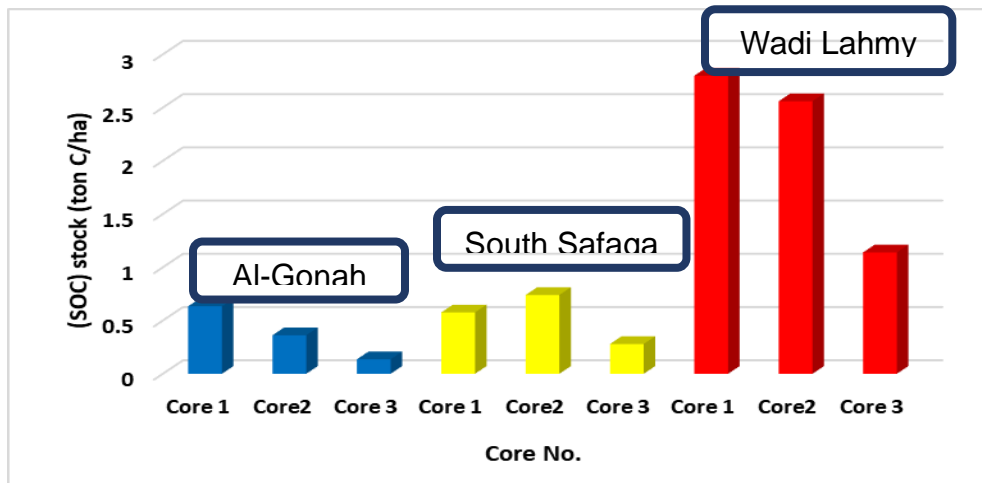


Fig.7. Average (SOC) stock in the sediment cores

Wadi Lahmy had a high average SOC content (2.16 ± 0.7 ton C/ ha) compared to Al-Gonah (0.37 ± 0.2 ton C/ ha) and South Safaga (0.5 ± 0.19 ton C/ ha). According to Table (7), the results of the classification of satellite images of the studied stations, Wadi Lahmy is dominated by dense vegetation (58%).

Table 7. Total area (hectares) of different vegetation classes in Al-Gonah, South Safaga, and Wadi Lahmy

Vegetation type/ station name	Shrub and grassland (hectare)	Sparse (hectare)	Dense (hectare)
Al-Gonah	2.25	0.54	0.09
South Safaga	1.08	1.35	0.45
Wadi Lahmy	4.77	4.5	12.69

In addition, a strong positive correlation was detected between SOC and vegetation density of the mangrove stand (0.99). It is worth noting that, the reference

core in the three stations has the lowest SOC stock. Thus, the mangrove sediment has a higher tendency to store carbon than the non-mangrove one. Mangroves have significantly different sediment SOC levels and dynamics, which are primarily controlled by the tidal gradient, mangrove forest age, biomass, and productivity, as well as species composition and suspended matter sedimentation (Meng *et al.*, 2022).

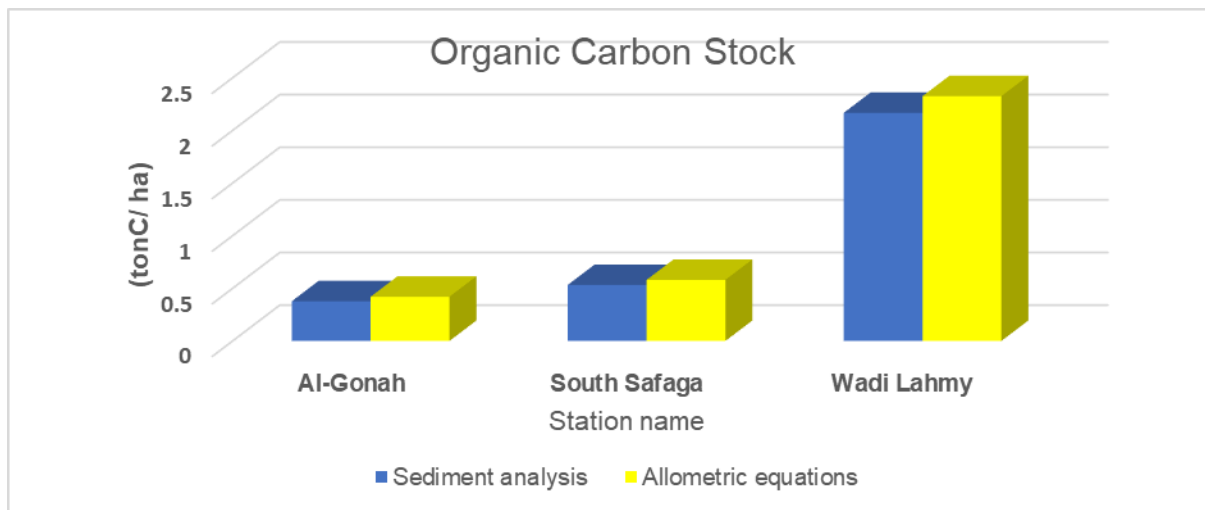


Fig. 8. Organic carbon stock estimates (ton C/ ha) for the 3 studied stations by applying two different methods for determination (Sediment analysis and allometric equations)

In the present study, the sediment analysis method was implemented to determine the SOC, as opposed to the allometric equation in the estimation of BGB for the 3 selected stations (Al-Gonah, South Safaga, and Wadi Lahmy). The results showed that the organic carbon stock estimate, obtained by applying the allometric method, is slightly higher than those obtained via the sediment analysis method with values of 9, 11, and 7% for Al-Gonah, South Safaga, and Wadi Lahmy, respectively (Fig. 8). This may be traced back to the overestimation of biomass for smaller mangrove stands, combined with lower vegetation density. Thus, the allometric equations remained one of the best ways for biomass prediction when combined with remote sensing data analysis albeit with considerable increases in prediction error, compared to the sediment analysis method.

4. Valuing the Red Sea (mangroves) blue carbon

The CO₂ sequestration potential (ton CO₂/ Landsat pixel) was employed to achieve the most accurate estimation of the carbon market for the Red Sea mangroves. The capacity of a mangrove plot/ pixel to sequester CO₂ was reclassified into three classes: rare, medium, and high. Hence, species composition, age, tree density, and size of the tree within the stand directly affect the biomass content and CSP (Figs. 9- 13).

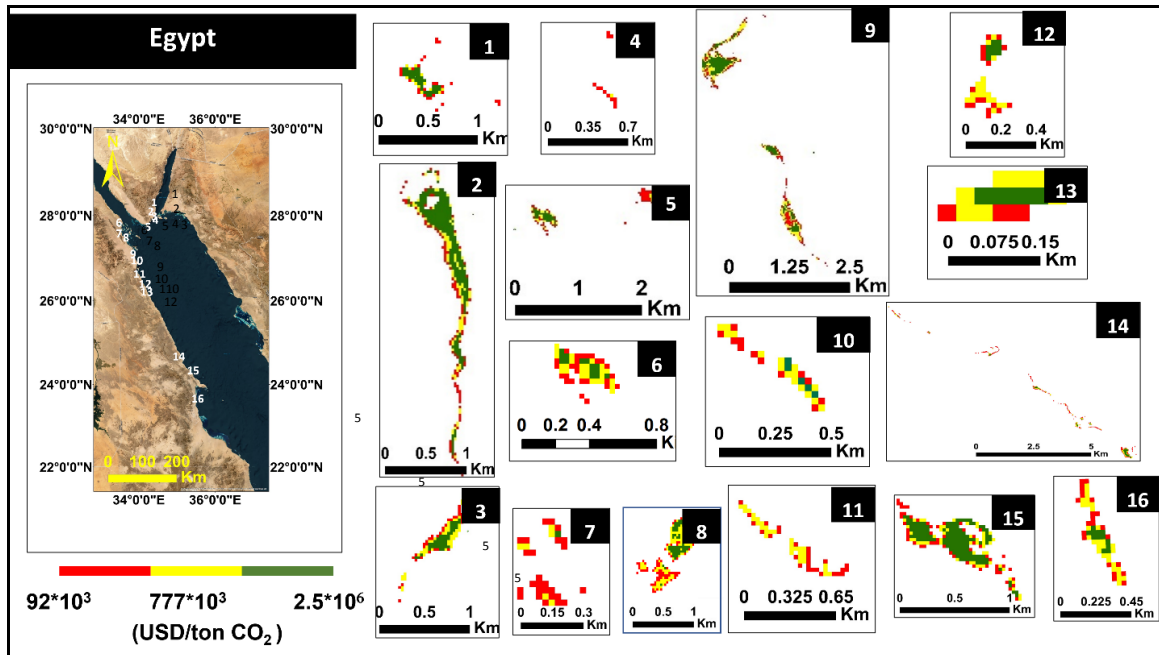


Fig. 9. Egypt zonation maps showing the USD/ ton and CO₂/ pixel of each mangrove stand detected in the present study

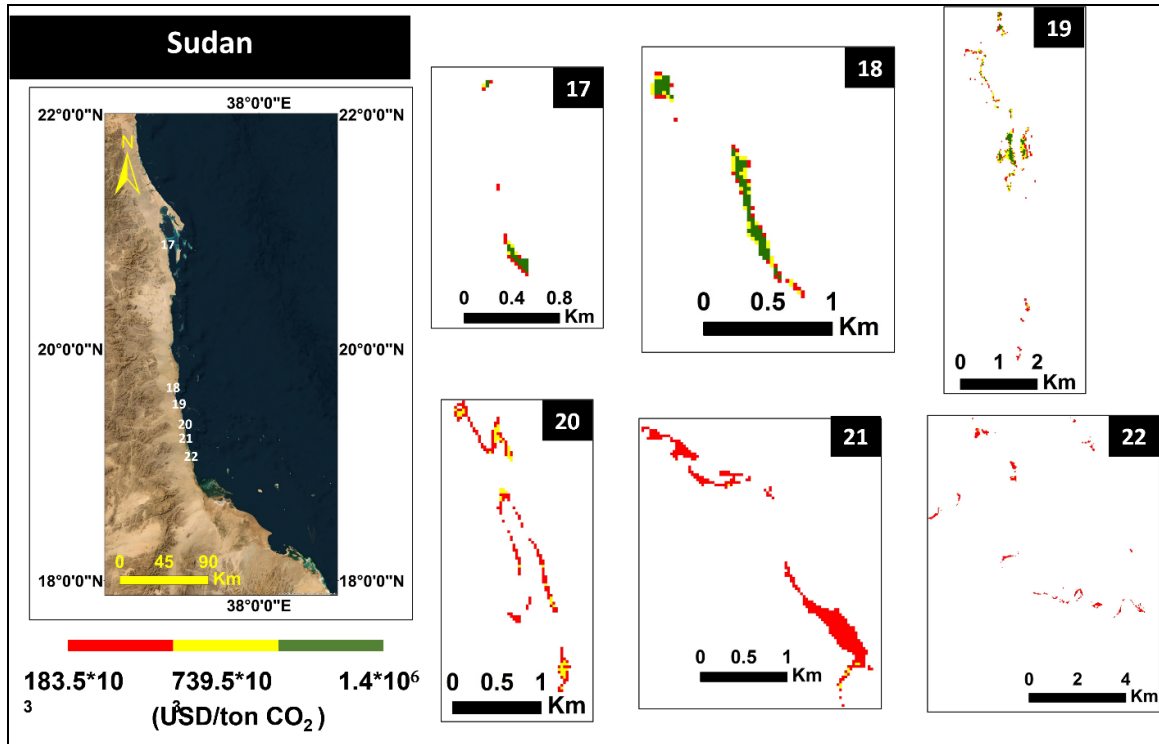


Fig. 10. Sudan zonation maps showing the USD/ ton and CO₂/ pixel of each mangrove stand detected in the present study

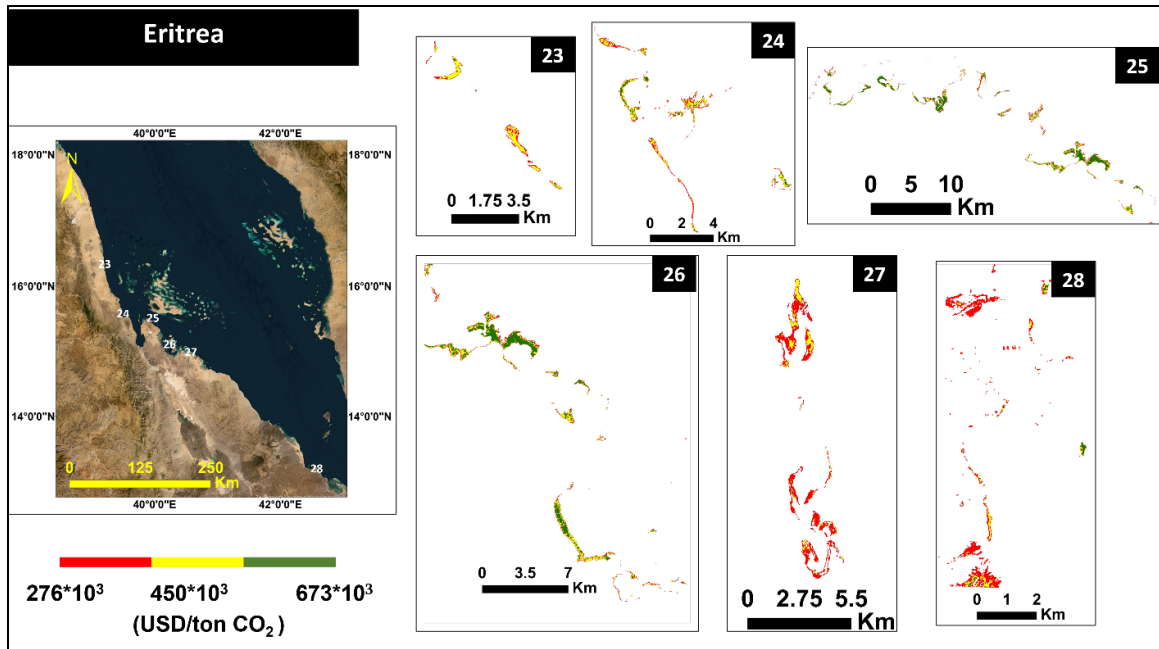


Fig. 11. Eritrea zonation maps showing the USD/ ton and CO₂/ pixel of each mangrove stand detected in the present study

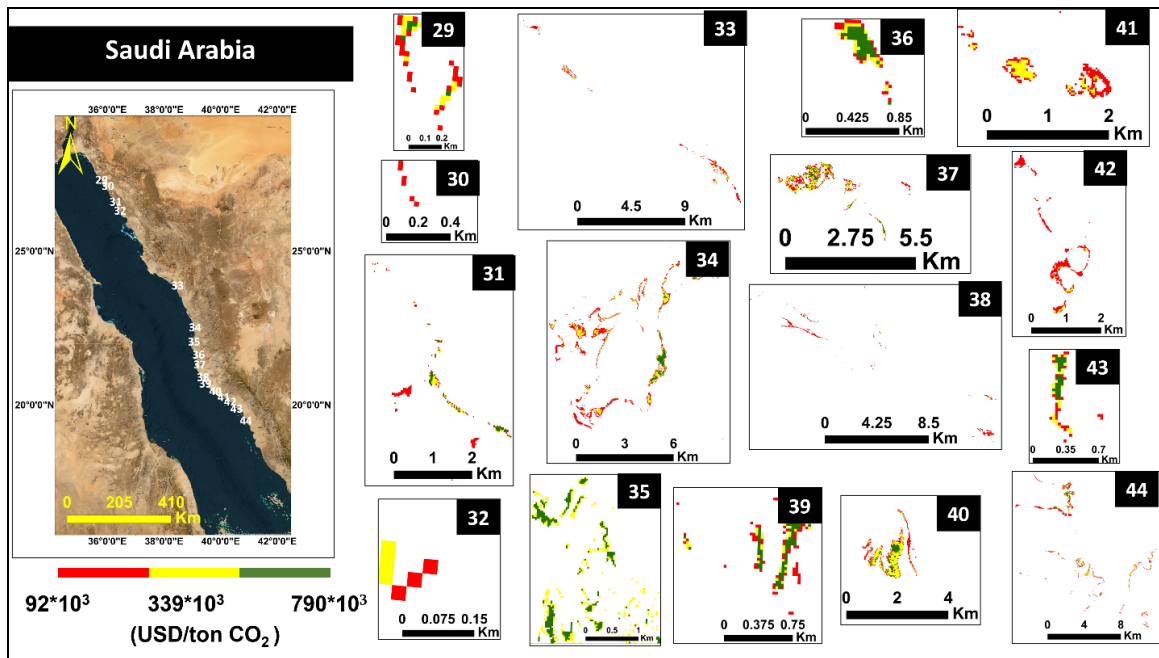


Fig. 12. Saudi Arabia zonation maps showing the USD/ ton and CO₂/ pixel of each mangrove stand detected in the present study

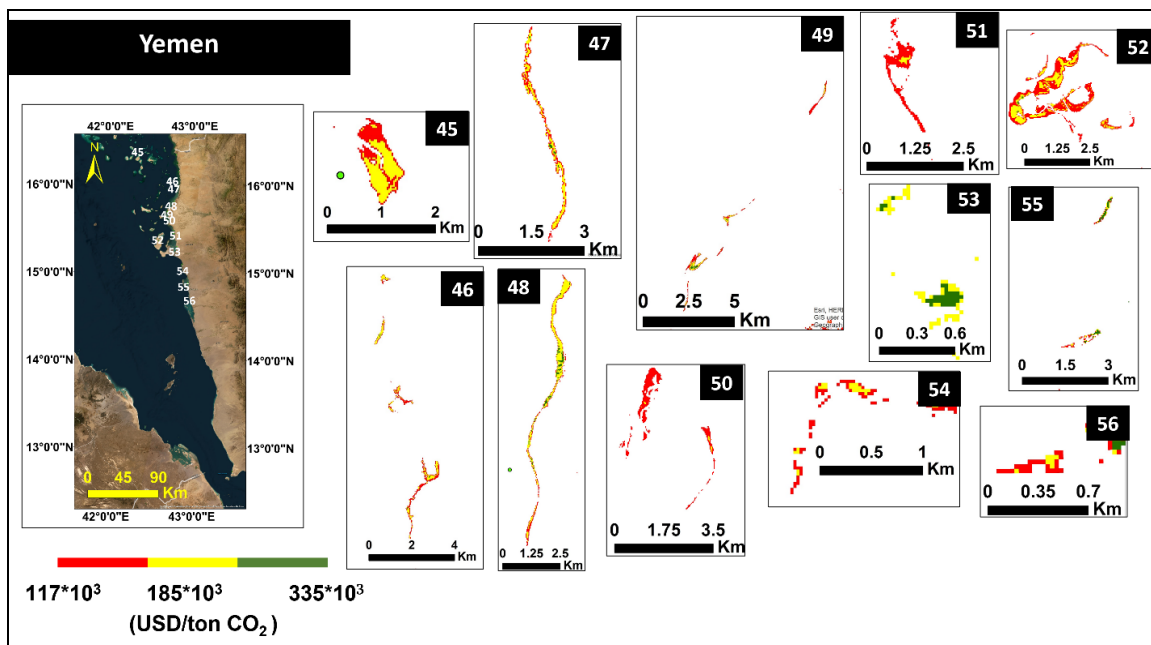


Fig. 13. Yemen zonation maps showing the USD/ ton and CO₂/ pixel of each mangrove stand detected in the present study

The maximum value of CO₂ sequestration potential of 561.4*10³ ton CO₂/ pixel was estimated in Egypt (station# 11-Wadi Abu Hamra), which may reflect the increase in dense mangrove cover. Conversely, the minimum value of ton CO₂/ landsat pixel (21.4*10³) was recorded in Saudi Arabia (station# 30-Duba). This might be related to the challenging environmental factors, such as the low rainfall and the arid climate.

Additionally, the Saudi Arabian Red Sea mangroves' ability to contribute to the carbon sequestration process is limited since the sediments are primarily consisting of biogenic carbonates (Almahasheer *et al.*, 2017).

Fig. (9) displays the USD/ ton and Co₂/ landsat pixel for each detected mangrove stand in the 5 studied countries. These places could be those with distinctive species/ genus assemblages, mangrove density or health, or even devastated areas. The information derived from the input of carbon sequestration potential per pixel was used to create a spectral differentiation that allowed for this.

Based on the price of voluntary carbon markets, this blue carbon stock potential might worth USD 4.3 ton⁻¹ CO₂ (Donofrio *et al.*, 2020). The Red Sea mangroves can share by at least USD 27.5M value of mangrove forests ecosystem services. This value could support the necessity for the conservation efforts to maintain the ongoing provision of ecosystem services and benefits. Although Egypt (station#8- Abu Minkar Island) wasn't proved to be the largest mangrove detected mangrove stand, it covers approximately 60 hectares. It recorded the maximum value of (CO₂) sequestration

potential/ pixel and shares by about USD 2.4 Mton⁻¹ CO₂/pixel. Given that the mangroves' location is in the center of the island and along a shallow channel, the area under study is exposed to regular tidal effects, soil accumulation, and continuous inundation. Furthermore, one of this area's characteristics is the presence of naturally growing and planted mangrove species. On the other hand, Saudi Arabia (station#3-Duba) showed the lowest CO₂ sequestration potential/ pixel (21*10³-ton CO₂/pixel), which is equivalent to USD 92*10³ ton⁻¹ CO₂/ pixel. According to **Shaltout *et al.* (2020)**, the northern locations of the Saudi Arabia coast are characterized by high salinity, relatively low temperatures, dry land, and minimal rainfall, which may adversely affect the density and presence of mangrove stands.

CONCLUSION

Accurate assessments of mangrove blue carbon stocks are crucial for climate change mitigation measures. However, maintaining carbon stock data across expansive and occasionally inaccessible mangrove forest areas is extremely difficult, especially in nations without national-scale management programs. In this regard, the integration of the remote sensing data, with the allometric equations, can help us move toward a more general and robust approach for estimating the carbon stock of mangrove forests, especially for large investigation areas such as the Red Sea. The results of the current study were validated by comparing them with other studies that employed the destructive method, and the comparison revealed that the results were acceptable and could be used to calculate the carbon content of *A. marina* in various mangrove environments. Thus, the present study opens the possibility for future research wherein the same technique can be applied to other areas.

Therefore, the current study offers up-to-date baseline information on the carbon content of *A. marina*, which will be highly helpful for future research including an ongoing monitoring of the ability of mangrove ecosystems to store carbon. The total carbon stock for the Red Sea mangroves was about 20 ton C/ ha, which is equivalent to 70.8 ton CO₂/ ha. If valued, the Red Sea mangrove blue carbon was estimated to worth USD 27.5M. From the aforementioned results, the Red Sea needs a comprehensive regional program for the restoration and rehabilitation of its mangrove to reach the optimum carbon sequestration potential and become an effective tool for climate change mitigation.

REFERENCES

Abohassan, R.; Okia, C.A.; Agea, J.G.; Kimondo, J.M. and McDonald, M.M. (2012). Perennial biomass production in arid mangrove systems on the Red Sea coast of Saudi Arabia. *J. Environ. Sci.*, 6: 22–31.

Afele, A. (2021). Linking Territorial and Coastal Planning: Conservation Status and Management of Mangrove Ecosystem at the Egyptian - African Red Sea Coast. *AUJES.*, 2(2): 91–114. <https://doi.org/10.21608/aujes.2021.65951.1013>

Afele, A.A.; Abbas, M.S.; Soliman, A.S.; Khedr, A.H.A. and Hatab, E.B.E. (2020). Tree biomass and soil carbon stocks of a Mangrove ecosystem on the Egyptian-African Red Sea coast. *Fundam. Appl. Limnol.* 193: 239–251. <https://doi.org/10.1127/fal/2020/1240>

Afele, A.A.; Abbas, M.S.; Soliman, A.S.; Khedr, A.H.A. and Hatab, E.-B.E. (2019). Physical and chemical characteristics of mangrove soil under marine influence. A case study on the Mangrove Forests at Egyptian-African Red Sea Coast. *Egypt. J. Aquat. Biol. Fish.* 23(3): 385 –399. <https://doi.org/10.21608/EJABF.2019.47451>

Ahmed, N., Glaser, M., 2016. Coastal aquaculture, mangrove deforestation and blue carbon emissions: Is REDD+ a solution? *Mar Policy* 66, 5866. <https://doi.org/10.1016/j.marpol.2016.01.011>

Aljenaid, S.; Abido, M.; Redha, G.K., AlKhuzaei, M.; Marsan, Y.; Khamis, A.Q.; Naser, H.; AlRumaidh, M. and Alsabbagh, M. (2022). Assessing the spatiotemporal changes, associated carbon stock, and potential emissions of mangroves in Bahrain using GIS and remote sensing data. *Reg Stud Mar Sci.* 52: 1–13. <https://doi.org/10.1016/j.rsma.2022.102282>

Almahasheer, H.; Aljowair, A.; Duarte, C.M. and Irigoien, X. (2016a). Decadal stability of Red Sea mangroves. *Estuar Coast Shelf Sci.* 169: 164–172. <https://doi.org/10.1016/j.ecss.2015.11.027>

Almahasheer, H., Duarte, C.M. and Irigoien, X. (2016b). Nutrient limitation in central red sea mangroves. *Front Mar Sci* 3. <https://doi.org/10.3389/fmars.2016.00271>

Almahasheer, H.; Serrano, O.; Duarte, C.M.; Arias-Ortiz, A.; Masque, P. and Irigoien, X. (2017). Low Carbon sink capacity of Red Sea mangroves. *Sci Rep.* 7(1): 9700–9709. <https://doi.org/10.1038/s41598-017-10424-9>

Arshad, M.; Alrumman, S.A. and Eid, E.M. (2018). Evaluation of carbon sequestration in the sediment of polluted and non-polluted locations of mangroves. *Fundam. Appl. Limnol.* 192, 53–64. <https://doi.org/10.1127/fal/2018/1127>

Berumen, M.L.; Voolstra, C.R. ; Daffonchio, D.; Agusti, S. M. ; Morán, J.G. and Duarte, C.M. (2019). The Red Sea: Environmental Gradients Shape a Natural Laboratory in a Nascent Ocean. In: “Coral reefs of the Red Sea.” Voolstra, C.R. and Berumen, M.L. (Eds). Springer Nature Switzerland, Switzerland, pp. 1–10. <https://doi.org/10.1007/978-3-030-0580296>

Blanco-Sacristán, J.; Johansen, K.; Duarte, C.M.; Daffonchio, D.; Hoteit, I. and McCabe, M.F. (2022). Mangrove distribution and afforestation potential in the Red Sea. *Sci. Total Environ.* 843(2):1–12. <https://doi.org/10.1016/j.scitotenv.2022.157098>

Cooray, L.I.G.; Kodikara, P.A.S.; Kumara, K.P.; Jayasinghe, M.I.; Madarasinghe, U.K.; Dahdouh-Guebas, S.; Gorman, F.; Huxham, D.; Jayatissa, M.P. and Jayatissa, L. P. (2021). Climate and intertidal zonation drive variability in the carbon stocks of Sri Lankan mangrove forests. *Geoderma.* 389: 1–13. <https://doi.org/10.1016/j.geoderma.2021.114929>

Curnick, D.; Pettorelli, N.; Amir, A.; Balke, T.; Barbier, E.; Crooks, S.; Dahdouh-Guebas, F.; Duncan, C.; Endors, C. and Friess, D. (2019). The value of small mangrove patches. *PLoS One.* 363: 239. <https://doi.org/10.1371/journal>

Donofrio, S.; Maguire, P.; Zwick, S. and Merry, W. (2020). Voluntary carbon and the post-pandemic recovery markets. A Special Climate Week NYC 2020 Installment of Ecosystem Marketplace's State of Voluntary Carbon Markets 2020 Report. Ecosystem Marketplace Insights Brief [Online]. Available: www.forest-trends.org

Dou, Z.; Cui, L.; Li, J.; Zhu, Y.; Gao, C.; Pan, X.; Lei, Y.; Zhang, M.; Zhao, X. and Li, W. (2018). Hyperspectral estimation of the chlorophyll content in short-term and long-term restorations of Mangrove in Quanzhou Bay Estuary, China. *Sustainability.* 10(14):1–15. <https://doi.org/10.3390/su10041127>

Eid, E.M.; El-Bebany, A.F. and Alrumman, S.A. (2016). Distribution of soil organic carbon in the mangrove forests along the southern Saudi Arabian Red Sea coast. *Rend. Lincei Sci.* 27: 629–637. <https://doi.org/10.1007/s12210-016-0542-6>

Eid, E.M.; Khedher, K.M.; Ayed, H.; Arshad, M.; Moatamed, A. and Mouldi, A. (2020). Evaluation of carbon stock in the sediment of two mangrove species, *Avicennia marina* and *Rhizophora mucronata*, growing in the Farasan Islands, Saudi Arabia. *Oceanologia.* 62: 200–213. <https://doi.org/10.1016/j.oceano.2019.12.001>

Eid, E.M. and Shaltout, K.H. (2016). Distribution of soil organic carbon in the mangrove *Avicennia marina* (Forssk.) Vierh. along the Egyptian Red Sea Coast. *Reg Stud Mar Sci.* 3: 76–82. <https://doi.org/10.1016/j.rsma.2015.05.006>

El-Hussieny, S.A. and Ismail, I.M. (2015). Role of *Avicennia marina* (Forssk.) Vierh. of South Sinai, Egypt in Atmospheric CO₂ Sequestration. *Int. J. Sci. Res.* 6: 1935–1943. <https://doi.org/10.21275/ART20171097>

Ellatif, A.A.A.; Merwad, A.M.A.; Moussa, K.F. and Abu-Hashim, M.S.D. (2022). Influence of mangrove ecosystem on soil carbon sequestration and global warming at the western strand of the Red Sea, Egypt. *Zagazig J. Agric. Res.* 49(4): 513-521.

Gao, T.; Ding, D.; Guan, W. and Liao, B. (2018). Carbon stocks of coastal wetland ecosystems on Hainan Island, China. *Pol J Environ Stud.* 27: 1061–1069. <https://doi.org/10.15244/pjoes/76501>

Hickey, S.M.; Callow, N.J.; Phinn, S.; Lovelock, C.E. and Duarte, C.M. (2018). Spatial complexities in aboveground carbon stocks of a semi-arid mangrove community: A remote sensing height-biomass-carbon approach. *Estuar Coast Shelf Sci.* 200: 194–201. <https://doi.org/10.1016/j.ecss.2017.11.004>

Hilmi, N.; Chami, R.; Sutherland, M.D.; Hall-Spencer, J.M.; Lebleu, L.; Benitez, M.B. and Levin, L.A. (2021). The Role of Blue Carbon in Climate Change Mitigation and Carbon Stock Conservation. *Front. Clim.* 3: 1 –18. <https://doi.org/10.3389/fclim.2021.710546>

Howard, J.; Hoyt, S.; Isensee, K.; Telszewski, M. and Pidgeon, E. (2014). Coastal Blue Carbon methods for assessing carbon stocks and emissions factors in mangroves, tidal salt marshes, and seagrass meadows. Arlington, Virginia, USA.

Intergovernmental Panel on Climate Change (IPCC). 2022. Framing and Context of the Report, in: *The Ocean and Cryosphere in a Changing Climate*. Pörtner, H.O. ; Roberts, D.C.; Masson-Delmotte, V.; Zhai, P.; Tignor, M.; Poloczanska, E.; Mintenbeck, K.; Alegría, A.; Nicolai, M.; Okem, A.; Petzold, J.; Rama, B. and Weyer, N.M. (eds.). Cambridge University Press, Cambridge, UK and New York, NY, USA, pp. 73–129. <https://doi.org/10.1017/9781009157964.003>

Intergovernmental Panel on Climate Change (IPCC). (2001). *CLIMATE CHANGE: THE SCIENTIFIC BASIS*. Contribution of Working Group I to the Third Assessment Report of the Intergovernmental Panel on Climate Change. Houghton, J.T.Y. ;Ding, D.J.; Griggs, M.; Noguer, P.J. ; van der Linden, X.; Dai, K.; Maskell, and C.A. Johnson (eds.). Cambridge University Press, Cambridge, United Kingdom and New York, NY, USA, 881pp.

Jaramillo, V.J.; Martínez-Yrizar, A. and Sanford, R.L. (2011). Primary Productivity and Biogeochemistry of Seasonally Dry Tropical Forests, in: *Seasonally Dry Tropical Forests*. Island Press/ Mar. Resour. Econ., pp. 109–128. https://doi.org/10.5822/978-1-61091-021-7_7

Jha, C.S.; Singh, S.; Gopalakrishnan, R. and Singh, S. (2015). Spatial Distribution of Biomass in Indian Forests Using Spectral Modelling Spectral and Spatial Indices based

Specific Class Identification from Airborne Hyperspectral Data View project. India. International Expert group Meeting on Geospatial Information Systems for Multi-scale Forest Biomass Assessment and Monitoring in the Hindu Kush-Himalayan Region At: ICIMOD, Kathmandu, Nepal. pp. 1–3.

Jones, A.R.; Raja Segaran, R.; Clarke, K.D.; Waycott, M.; Goh, W.S.H. and Gillanders, B.M. (2020). Estimating Mangrove Tree Biomass and Carbon Content: A Comparison of Forest Inventory Techniques and Drone Imagery. *Front Mar Sci* 6: 1–13. <https://doi.org/10.3389/fmars.2019.00784>

Kauffman, J.B. and Cole, T.G. (2010). Micronesian mangrove forest structure and tree responses to a severe typhoon. *Wetlands* 30, 1077–1084. <https://doi.org/10.1007/s13157-010-0114-y>

Kauffman, J.B. and Donato, D.C. (2012). Working Paper Protocols for the measurement, monitoring and reporting of structure, biomass and carbon stocks in mangrove forests. Indonesia. Center for International Forestry Research. pp. 40.

Khalil, A.S.M. (2015). Mangroves of the Red Sea. pp. 585–597. https://doi.org/10.1007/978-3-662-45201-1_33

Khan, K.; Iqbal, J.; Ali, A. and Khan, S.N. (2020). Assessment of sentinel-2-derived vegetation indices for the estimation of above-ground biomass/carbon stock, temporal deforestation and carbon emissions estimation in the moist temperate forests of Pakistan. *Appl Ecol Environ Res* 18, 783–815. https://doi.org/10.15666/aeer/1801_783815

Komiyama, A.; Ong, J.E. and Pongparn, S. (2008). Allometry, biomass, and productivity of mangrove forests: A review. *Aquat Bot.* 89 (2): 128–137. <https://doi.org/10.1016/j.aquabot.2007.12.006>

Kovacs, J.M.; Flores-Verdugo, F.; Wang, J. and Aspden, L.P. (2004). Estimating leaf area index of a degraded mangrove forest using high spatial resolution satellite data. *Aquat Bot* 80, 13–22. <https://doi.org/10.1016/j.aquabot.2004.06.001>

Lin, W.T.; Lin, C.Y. and Chou, W.C. (2006). Assessment of vegetation recovery and soil erosion at landslides caused by a catastrophic earthquake: A case study in Central Taiwan. *Ecol Eng* 28, 79–89. <https://doi.org/10.1016/j.ecoleng.2006.04.005>

López, G.I. (2017). Grain Size Analysis. In: Gilbert, A.S. (eds) *Encyclopedia of Geoarchaeology*. Encyclopedia of Earth Sciences Series. Springer, Dordrecht. pp. 341–348. https://doi.org/10.1007/978-1-4020-4409-0_18

Madkour, H.A. and Mohammed, A.W. (2008). Nature and geochemistry of surface sediments of the mangrove environment along the Egyptian Red Sea coast. *Environmental Geology* 54, 257–267. <https://doi.org/10.1007/s00254-007-0813-8>

Mashaly, I.A.; Hegazy, A.K.; Aal, M.A. and El-Hussieny, S.A. (2016). Habitat-Based Estimate of Carbon Content in Mangrove *Avicennia marina* (Forssk.) Vierh. of South Sinai, Egypt. *IOSR Journal of Environmental Science* 10, 8–14. <https://doi.org/10.9790/2402-1011020814>

Meng, Y.; Bai, J.; Gou, R.; Cui, X.; Feng, J.; Dai, Z.; Diao, X.; Zhu, X. and Lin, G. (2021). Relationships between above- and below-ground carbon stocks in mangrove forests facilitate better estimation of total mangrove blue carbon. *Carbon Balance Manag* 16, 1–14. <https://doi.org/10.1186/s13021-021-00172-9>

Meng, Y.; Gou, R.; Bai, J.; Moreno-Mateos, D.; Davis, C.C.; Wan, L.; Song, S.; Zhang, H.; Zhu, X. and Lin, G. (2022). Spatial patterns and driving factors of carbon stocks in mangrove forests on Hainan Island, China. *Global Ecology and Biogeography* 31, 1692–1706. <https://doi.org/10.1111/geb.13549>

Cairns, M.A.; Brown, S. ; Helmer, E.H. and Baumgardner, G.A. (1997). Root biomass allocation in the world's upland forests. *Oecologia* 111, 1–11.

Palacios Peñaranda, M.L.; Cantera Kintz, J.R. and Peña Salamanca, E.J. (2019). Carbon stocks in mangrove forests of the Colombian Pacific. *Estuar Coast Shelf Sci* 227. <https://doi.org/10.1016/j.ecss.2019.106299>

Panda, S.S.; Ames, D.P. and Panigrahi, S. (2010). Application of vegetation indices for agricultural crop yield prediction using neural network techniques. *Remote Sens (Basel)* 2, 673–696. <https://doi.org/10.3390/rs2030673>

Situmorang, J. P.; Sugianto, S.D. and Darusman, D. (2016). Estimation of Carbon Stock Stands using EVI and NDVI Vegetation Index in Production Forest of Lembah Seulawah Sub-District, Aceh Indonesia. *Aceh International Journal of Science and Technology* 5(3):126 –139. <https://doi.org/10.13170/aijst.5.3.5836>

PERSGA/GEF (2004). The Regional Organization for the Conservation of the Environment of the Red Sea and Gulf of Aden Status of Mangroves in the Red Sea and Gulf of Aden. PERSGA Technical Series No. 11. pp. 260.

Hastuti, W.A.; Suniada, I.K. and Islamy, F. (2017). Carbon stock estimation of mangrove vegetation using remote sensing in Perancak Estuary, Jembrana District, Bali, nt J Remote Sens. 14(2): 137 –150. <https://doi.org/10.30536/j.ijreses.2017.v14.a2841>

Hogarth, P.J. (2002). The Biology of Mangroves . Biology of Habitats. Q Rev Biol 77, 43–111. <https://doi.org/10.1086/343660>

Pham, L.T.H. and Brabyn, L. (2017). Monitoring mangrove biomass change in Vietnam using SPOT images and an object-based approach combined with machine learning algorithms. ISPRS Journal of Photogrammetry and Remote Sensing 128, 86–97. <https://doi.org/10.1016/j.isprsjprs.2017.03.013>

Pizaña, J.M.G.; Hernández, J.M.N. and Romero, N.C., 2016. Remote Sensing-Based Biomass Estimation, in: Environmental Applications of Remote Sensing. InTech. Pp. 1–40. <https://doi.org/10.5772/61813>

Rasquinha, D.N. and Mishra, D.R. (2021). Impact of wood harvesting on mangrove forest structure, composition and biomass dynamics in India. Estuar Coast Shelf Sci 248. <https://doi.org/10.1016/j.ecss.2020.106974>

Rosenqvist, A.; Shimada, M.; Suzuki, S.; Ohgushi, F.; Tadono, T.; Watanabe, M.; Tsuzuku, K.; Watanabe, T.; Kamijo, S. and Aoki, E. (2014). Operational performance of the ALOS global systematic acquisition strategy and observation plans for ALOS-2 PALSAR-2. Remote Sens Environ 155, 3–12. <https://doi.org/10.1016/j.rse.2014.04.011>

Ross, M.S.; Ruiz, P.L.; Telesnicki, G.J. and Meeder, J.F. (2001). Estimating above-ground biomass and production in mangrove communities of Biscayne National Park, Florida (U.S.A.), Wetlands Ecology and Management.

Rovai, A.S.; Coelho-Jr, C.; de Almeida, R.; Cunha-Lignon, M.; Menghini, R.P.; Twilley, R.R.; Cintrón-Molero, G. and Schaeffer-Novelli, Y. (2021). Ecosystem-level carbon stocks and sequestration rates in mangroves in the Cananéia-Iguape lagoon estuarine system, southeastern Brazil. For Ecol Manage 479. <https://doi.org/10.1016/j.foreco.2020.118553>

Saenger, P. and Snedaker, S.C. (1993). Pantropical trends in mangrove above-ground biomass and annual litterfall, Oecologia.

Santos, I.R.; Burdige, D.J.; Jennerjahn, T.C.; Bouillon, S.; Cabral, A.; Serrano, O.; Wernberg, T.; Filbee-Dexter, K.; Guimond, J.A. and Tamborski, J.J. (2021). The renaissance of Odum’s outwelling hypothesis in “Blue Carbon” science. Estuar Coast Shelf Sci 255. <https://doi.org/10.1016/j.ecss.2021.107361>

Senger, D.F.; Saavedra Hortua, D.A.; Engel, S.; Schnurawa, M.; Moosdorf, N. and Gillis, L.G. (2021). Impacts of wetland dieback on carbon dynamics: A comparison between intact and degraded mangroves. Science of the Total Environment 753. <https://doi.org/10.1016/j.scitotenv.2020.141817>

Shaltout, K.H.; Ahmed, M.T.; Alrumman, S.A.; Ahmed, D.A. and Eid, E.M. (2020). Evaluation of the carbon sequestration capacity of arid mangroves along nutrient availability and salinity gradients along the Red Sea coastline of Saudi Arabia. *Oceanologia* 62, 56–69. <https://doi.org/10.1016/j.oceano.2019.08.002>

Sidi, A.A.; Okunlola, L.A. and Waziri, N.M. (2023). Organic Carbon (OC) and Organic Matter (OM) in Sediments Collected from Two Wetlands in Central Bida Basin, Nigeria. *J. geosci. environ. Prot.* 11, 218-226. <https://doi.org/10.4236/gep.2023.1110015>

Soares, M.L.G., Schaeffer-Novelli, Y. (2005). Above-ground biomass of mangrove species. I. Analysis of models. *Estuar Coast Shelf Sci* 65, 1–18. <https://doi.org/10.1016/j.ecss.2005.05.001>

Subasinghe, U.; Subasinghe, S. and Harpriya, A., 2014. Prediction of Stem Biomass of *Pinus caribaea* Growing in the Low Country Wet Zone of Sri Lanka Agarwood resin formation View project Forest Tree Biomass and Carbon View project Prediction of Stem Biomass of *Pinus caribaea* Growing in the Low Country Wet Zone of Sri Lanka. *Journal of Tropical Forestry and Environment* 4, 40–49. <https://doi.org/10.13140/2.1.4645.6967>

Suwa, R., Rollon, R., Sharma, S., Yoshikai, M., Albano, G.M.G., Ono, K., Adi, N.S., Ati, R.N.A., Kusumaningtyas, M.A., Kepel, T.L., Maliao, R.J., Primavera-Tirol, Y.H., Blanco, A.C., Nadaoka, K. (2021). Mangrove biomass estimation using canopy height and wood density in the South East and East Asian regions. *Estuar Coast Shelf Sci* 248. <https://doi.org/10.1016/j.ecss.2020.106937>

Taillardat, P.; Friess, D.A. and Lupascu, M. (2018). Mangrove blue carbon strategies for climate change mitigation are most effective at the national scale. *Biol Lett* 14. <https://doi.org/10.1098/rsbl.2018.0251>

Vaghela, B.; Chirakkal, S.; Putrevu, D. and Solanki, H. (2021). Modelling above ground biomass of Indian mangrove forest using dual-pol SAR data. *Remote Sens Appl* 21. <https://doi.org/10.1016/j.rsase.2020.100457>

Wang, L.; Jia, M.; Yin, D. and Tian, J. (2019). A review of remote sensing for mangrove forests: 1956–2018. *Remote Sens Environ.* 231:1 –15. <https://doi.org/10.1016/j.rse.2019.111223>

Wasserman, J.; Human, L.R.D. and Adams, J.B. (2023). Blue carbon stocks in southern Africa's Endangered seagrass *Zostera capensis*. *Estuar Coast Shelf Sci.* 284:1–15. <https://doi.org/10.1016/j.ecss.2023.108296>

Westlake, D.F., 1963. Comparisons of plant productivity. *Bid. Rev.* 83: 285–425.

Wijeyaratne, W.M.D.N. and Liyanage, P.M. (2022). Development of allometric equations to estimate the stem carbon content of *Lumnitzera racemosa* and *Avicennia marina* in a tropical mangrove ecosystem: A novel non-destructive approach. *Acta Ecol. Sin.* 42: 95–100. <https://doi.org/10.1016/j.chnaes.2021.08.012>

Wilke, B.-M. (2005). Determination of Chemical and Physical Soil Properties, in: Margesin, R., S.F. (Ed.), *Manual for Soil Analysis-Monitoring and Assessing Soil Bioremediation*. Springer-Verlag, Heidelberg, pp. 47–95.

Wilson, M.S.; van Beynen, P.; Rains, M. and Hafen, M. (2009). Development of a Mangrove Quality Index in Tampa Bay, Florida. MSc. Thesis, Department of Geography, College of Arts and Sciences, University of South Florida. pp. 92.

Xu, M.; Sun, C.; Du, Z. and Zhu, X. (2023). Impacts of aquaculture on the area and soil carbon stocks of mangrove: A machine learning study in China. *Sci Total Environ.* 859:1–11. <https://doi.org/10.1016/j.scitotenv.2022.160173>

Yue, J.W.; Guan, J.H.; Deng, L.; Zhang, J.G.; Li, G. and Du, S. (2018). Allocation pattern and accumulation potential of carbon stock in natural spruce forests in northwest China. *PeerJ.* 1: 15–35. <https://doi.org/10.7717/peerj.4859>